

## DAMPING CHARACTERISTICS OF RC SHEAR WALL IN THE WEAK NONLINEAR RANGE

Katsuya IGARASHI<sup>1</sup>

### SUMMARY

A precise static loading test on a reinforced concrete shear wall (RC) having an I-shaped section and a low aspect ratio was conducted to investigate its fundamental characteristics such as its restoring force relationship and equivalent damping ratio in the weak plastic range. The following conclusions are obtained:

- (1) it is important to measure the strain in the reinforcing bars and the displacement around the bottom of the flange wall to precisely evaluate the flexure displacement,
- (2) equivalent damping is very small: 0.5% for flexure deformation and 1.5% for shear deformation.

### INTRODUCTION

It is well known that the fundamental characteristics of RC shear walls, such as stiffness, shear capacity and damping factor, are affected by loading rate and exposed displacement magnitude. The dynamic and static characteristics in the strong nonlinear range have become increasingly clear, recently [Okada et al, 1988,1989], [Shibata et al, 1990, 1993, 1995], [Sakai et al, 1992], [Kanechika et al, 1997], [Muroi et al, 1997].

In structural design, it is important to know the characteristics in the weak nonlinear range, but previous researches have mainly focused on the final destructive stage or the seismic margin. As a result, insufficient information is available on the weak nonlinear range.

Therefore, static and dynamic loading tests on RC shear walls were conducted to investigate their fundamental characteristics, focusing on the weak nonlinear range such as stiffness and damping factor. This paper discusses only the static test results.

## 2. TEST METHOD

### 2.1 Specimen

The test specimen was a RC shear wall model as shown in Figure 1. It had an I shaped section, a low aspect ratio of 0.8, a steel reinforcement ratio of 1.2% and the same dimensions as in the literature [Shibata and et al, 1990, 1993, 1995].

A steel weight of 107.9kN was loaded on the top slab of the specimen to realize the same test setup configuration as the dynamic test. The average axial stress in the wall was 1.27 kN/mm<sup>2</sup>.

Normal ready mixed concrete with a maximum aggregate size of 25mm was used for the base and top slab. Mortar with a maximum aggregate size of 5mm was used for the wall. Specially made D3 bars at 45mm interval were used for the wall reinforcement.

The specimen's material properties and fundamental characteristics calculated from JEAG's formula [JEAG, 1991] are listed in Table 1 and Table 2, respectively.

### 2.2 Loading Method

The specimen fixed on the reaction floor and the test setup are shown in Photo1. In this test, a specially made precise screw jack driven by an AC servomotor was used instead of the conventional oil jack to improve the

<sup>1</sup> Kajima Technical Research Institute, Kajima Corporation, Japan, E-mail : igarashi@katri.kajima.co.jp

loading accuracy. The jack's minimum resolution was about 98N. A load was applied to both sides (parallel to the loading direction) of the top slab through the steel beams, which were bolted to the specimen as seen in Photo 1. The maximum load applied to the specimen was increased from  $\pm 9.8\text{kN}$  to  $\pm 156.9\text{kN}$  in  $19.6\text{kN}$  steps. Each step consisted of 4 cycles. The first cycle was a transient loop, and 100% of the target load was applied to the specimen. The other 3 cycles were stable loops, where 90% of the first cycle load was applied to the specimen.

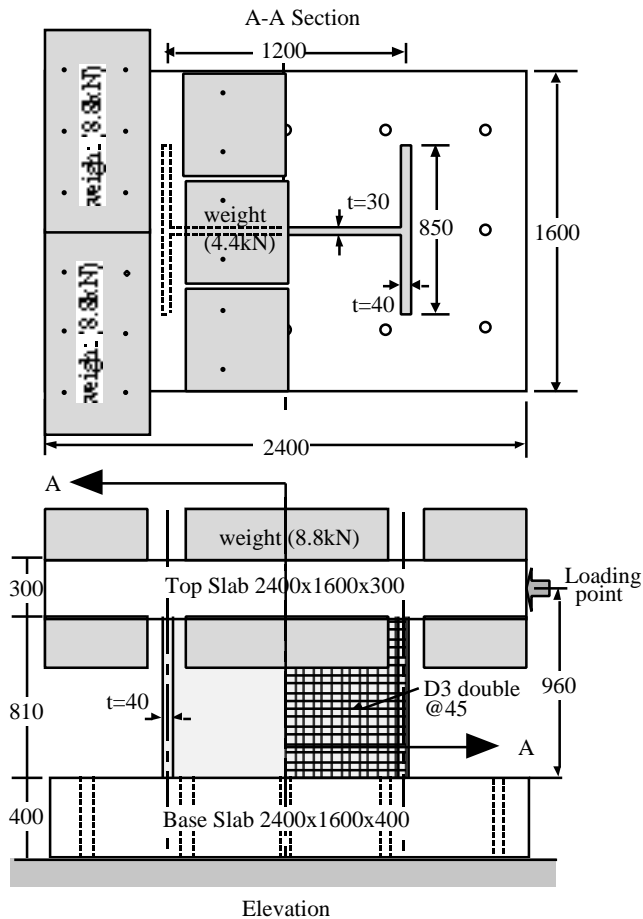


Figure 1: Detail of Specimen

Table 1 : Material Characteristics of Specimen

Reinforcement		
Young's Modulus (GPa)	Yield Strength (MPa)	Tensile Strength (MPa)
205.9	323.5	420.0
Concrete		
Young's Modulus (GPa)	Compressive Strength (MPa)	Split Tensile Strength (MPa)
21.9	39.5	3.3

Table 2: Calculated Structural Characteristics of Specimen

Items	Obtained Values	Drift Angle*
Flexure Stiffness	2411.6(kN/mm)	/
Shear Stiffness	475.5(kN/mm)	
Total Stiffness	397.2(kN/mm)	
Load at Shear Crack	91.9(kN)	0.23/1000
Disp at Shear Crack	0.19(mm)	
Load at Second Break Point	124.1(kN)	0.70/1000
Disp at Second Break Point	0.57(mm)	
Load at Flexure Crack	231.6(kN)	0.1/1000
Disp at Flexure Crack	0.096(mm)	

\*: Shear disp was divided by clear height  
Flexure disp was divided by Loading point height



Photo1: Specimen and Test Setup

### 2.3 Measurements and Data Reduction

Measurements were conducted of load, displacements and strain of the steel reinforcement. The applied load was measured by load cell, the horizontal displacement of the specimen was measured by the non-contacting displacement meters ( $\pm 2.5\text{mm}$ ), the vertical expansion or contraction of the flange wall was measured by the LVDTs ( $\pm 1\text{mm}$ ), and the strains in the reinforcing bars were measured by strain gauges.

The measured displacement was processed and separated into components according to the procedure shown in Figure 2. An average curvature ( $\phi_i$ ) of that section was estimated from the vertical expansion or contraction displacement ( $\Delta X_i$ ) of each measuring section of the flange wall as shown in Figure 2. Flexure displacement called the apparent flexure displacement ( $\delta_B$ ) was calculated by integrating the average curvature of each section from the bottom to the top of the wall. Shear displacement ( $\delta_S$ ) was obtained by subtracting the apparent flexure displacement from the measured horizontal displacement ( $\delta_T$ ). The apparent flexure displacement includes that caused by pulling out of the reinforcement at the bottom of the flange wall. To discuss the flexure displacement in detail, the contribution of the base rotation is excluded. This is called flexure displacement without rotation ( $\delta_F$ ).

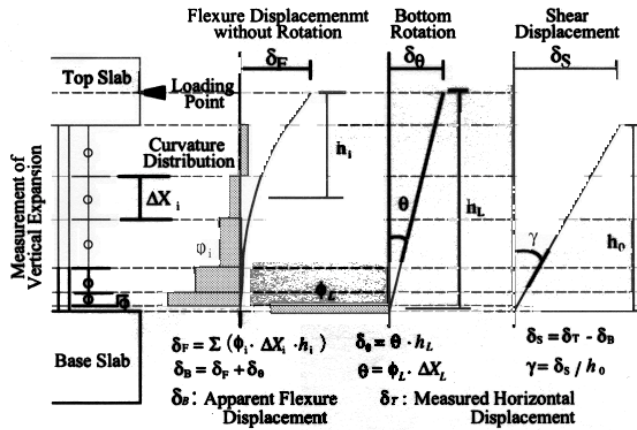


Figure 2: Method to Separate Measured Displacement to Each Component

While assuming a triangular curvature distribution the same as a cantilever beam, the contribution of the vertical displacement in the upper part of the wall is very small to the total flexure displacement, so precise measurement on vertical displacement is not done. However, the effect of inverse bending caused by the thick upper slab to the curvature distribution is not negligible. An FEM analysis is conducted to determine the most suitable position of the instruments. The following conclusions were obtained from the analysis.

- (1) The curvature beneath the upper slab is more than -30% of that of the top of the base slab caused by inverse bending of the top slab, as shown in Figure 3-(a). However, the effect of bending back is very small: only -1% of the total flexure displacement.
- (2) The flexure displacement without rotation ( $\delta_F$ ) caused by curvature at the bottom of the wall accounts for a larger percentage of the apparent flexure displacement ( $\delta_B$ ) because of its long arm, as shown in Figure 3-(b). For 4 points measurement, as seen in the literature [Okada et al, 1989], it is 25%, but for 6 points measurement, decreases to 10%. In actual measurement, the displacement caused by pullout of the reinforcement becomes incorporated into the measured displacement at the bottom of the wall, so it is strongly recommended to make a measurement as close as possible to the bottom of the wall to reduce its effect.

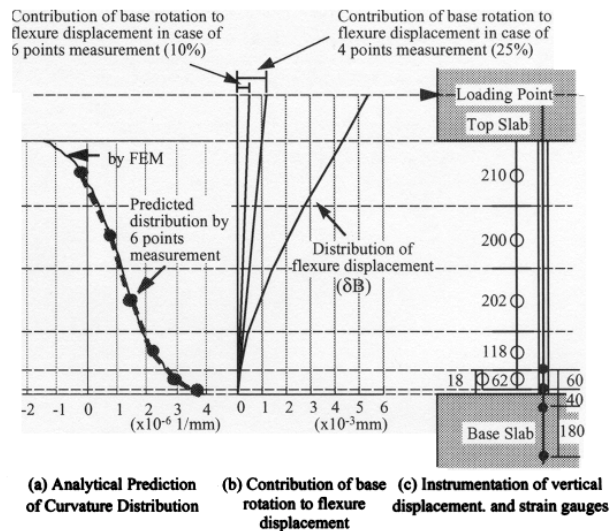


Figure 3 : Distribution of Curvature and Flexure Displacement and Instrumentations on Flange Wall

Based on the above results, the arrangement of instruments for vertical expansion was determined as shown in Figure 3-(c). To discuss the elongation of the reinforcement at the bottom of the flange wall in detail, four strain

gauges were glued to each reinforcing bar in the flange wall. Two gauges were glued above the surface of the base slab, corresponding to the position of the vertical displacement measurement, and two were glued inside the base slab as shown in Figure 3-(c). In addition, to detect shear cracks in the web wall, six gauges were glued to the two lateral reinforcing bars (three gauges to each).

### 3. TEST RESULTS

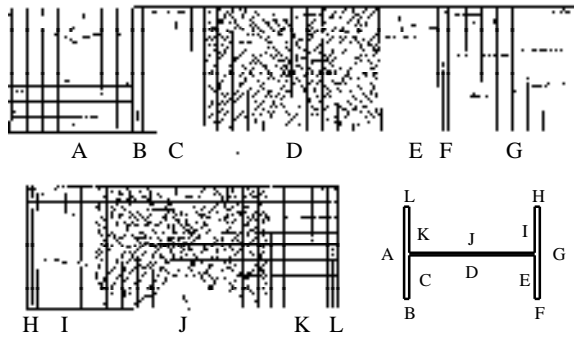


Figure 4: Crack Pattern after Test

In this test, a load was applied continuously up to  $\pm 156.9\text{kN}$  with a short stop during the data acquisition. Crack observation for the walls was conducted after the test, not during loading. The final crack pattern of the specimen is shown in Figure 4. Load versus total displacement and the apparent flexure displacement ( $\delta_{F+}$ ) relationships are shown in Figure 5, and load versus shear displacement and flexure displacement without rotation ( $\delta_F$ ) relationships are shown in Figure 6. It is clearly seen from the load displacement relationship and the load strain of lateral reinforcement relationship that the specimen remains in the elastic stage up to  $39.2\text{kN}$ . It is assumed that shear cracks occurred and spread into the web wall, where the applied load is  $56.8$  to  $75.5\text{kN}$ . That is  $60$  to  $80\%$  of the calculated shear crack load listed in Table 2.

Loops of load versus apparent flexure displacement have some area even in the small load range. However load versus flexure displacement without rotation curves has an almost linear relationship up to  $100\text{kN}$ . This implies that most of the energy dissipation in the load-apparent flexure displacement relationship occurs at the bottom of the wall, caused by pulling out of the reinforcement, and the rest of the flange wall remains in the elastic range. This tendency is also explained by the crack distribution in the specimen, such as many shear cracks in the web wall and small cracks in the flange wall as shown in Figure 4.

### 4. DISCUSSION

#### 4.1 Load Deflection Relationship

The left-hand side of Figure 7 shows the load versus the ratio of each separated displacement component, which is estimated by picking up the apexes of loops from Figures 5 and 6. The ratio estimated by FEM is shown in the same figure. The ratio of the shear displacement is about  $80\%$  up to  $60\text{kN}$  of load, and is assumed to be in the elastic range. This number matched well with the analytically predicted value of  $81\%$ . The ratio of the rotational displacement caused by pulling out at the bottom of the wall does not fluctuate so much, ranging from  $10\%$  to  $15\%$ .

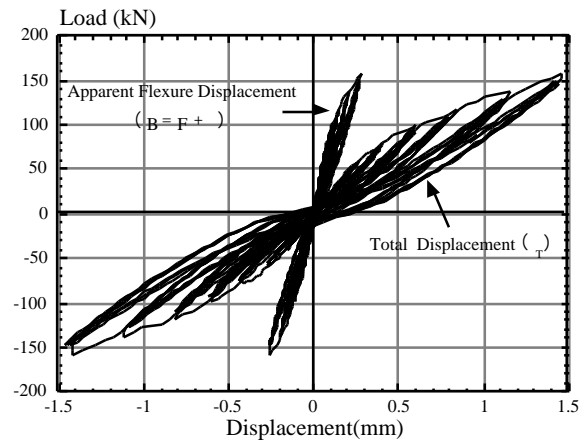


Figure 5: Load Displacement Curves (Total and Apparent Flexure)

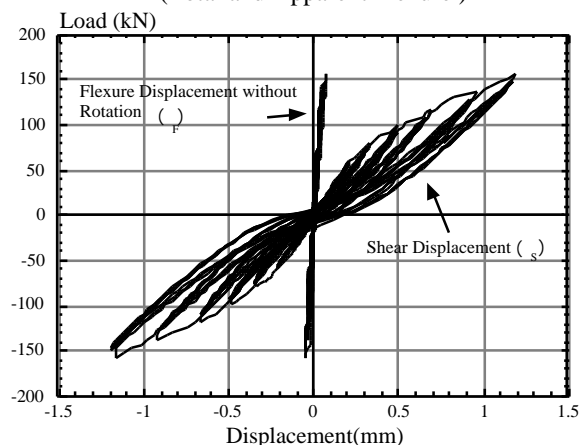


Figure 6: Load Displacement Curves (Flexure without Rotation and Shear)

The right hand of Figure 7 shows the load versus the ratio of shear displacement and compensated flexure displacement. The compensated flexure displacement is obtained by adding the contribution of the bottom of the wall, which is estimated from FEM analysis to be about 10% of the total flexure displacement, to the flexure displacement without rotation. The ratio of shear displacement increases to 87%, which is larger than the analytical value of 81%.

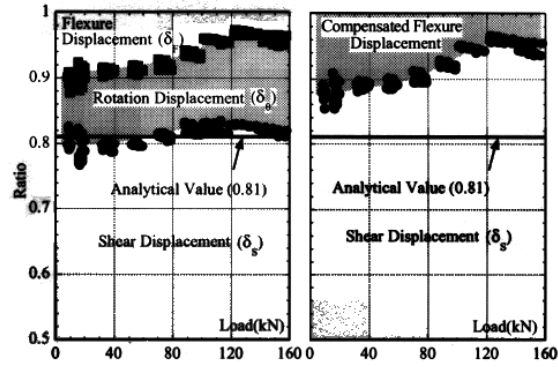


Figure 7 : Ratio of Separated Displacement

The left-hand side of Figure 8 shows the curvature distribution along the height of the specimen. The solid line represents the analytical value and the others the experimental results in the elastic range where the loads are less than 60kN. All data are normalized by the applied load and presented data per unit load of 9.8kN. The curvature of the bottom of the wall is extraordinarily larger than the analytical value, but the other parts except the top correspond closely to the analytical results. The negative curvature at the top of the wall is from 10 to 20 times larger than the analytical value because of the inverse bending caused by the thick top slab.

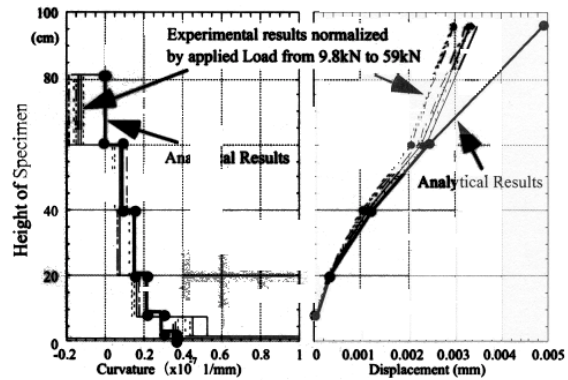


Figure 8 : Distribution of Curvature and Flexure Displacement

The right hand side of Figure 8 shows the distribution of flexure displacement without rotation along the height of the specimen, which is also normalized by the applied load. Up to the mid-height of the specimen, the experimental results correspond closely to the analytical values, but at the top, because of the inverse bending, flexure displacements are smaller than the analytical values.

The loading condition is different from the analysis in the actual experiment, because of the inverse bending effect caused by the thick top slab. Therefore, the magnitude of flexure displacement becomes smaller as the ratio of shear displacement becomes large compared with the analytical prediction, as seen on the right hand side of Figures 7 and 8.

#### 4.2 Comparison of Curvature with Strain of Reinforcing bars at the bottom of the flange wall

Strain gauges were glued on the vertical reinforcement of the flange wall. Their positions corresponded to those of the flexure displacement at the bottom of the flange wall, as shown in Figure 3(c), so it is possible to compare the curvature obtained from vertical displacement with that from the strain gauge readings. Measured data at e3, which was 200mm beneath the surface of the base slab, were very small, so point e3 is assumed to be fixed.

Strain in reinforcement around the bottom of the flange wall is measured at two points. One is deep in the base slab, and the other is 20 mm above the surface of the slab. These are denoted by e3 and e1, respectively as shown in Figure 9.

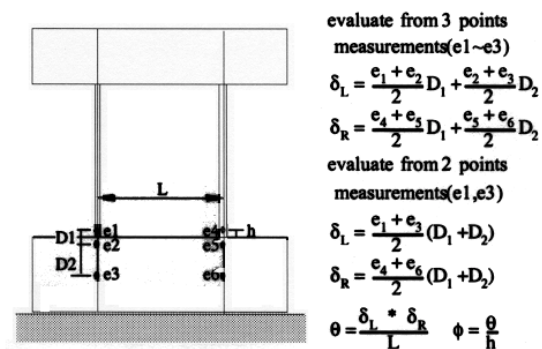


Figure 9 : Method to Estimate a Curvature from Strain

The curvature so estimated at those two points, i.e., by the conventional method, are smaller than that obtained from the vertical displacement at the bottom of the wall. Another new method is to add one point (e2) between

e1 and e3, and estimate the curvature from data of these three points. Results from this method are compared with those obtained from the conventional method shown on the right hand side of Figure 9. Results obtained from the experiment, the conventional and the new method in the elastic range are compared in Table 3.

Values estimated by the conventional method range from 35% to 66% of the experimental results, and average just 44%. However, the values estimated by the new method range from 88% to 144%, and average 101%. In the nonlinear range where the applied load is more than 60kN, the values estimated by the new method range over more than 80%. From these results, it is concluded that the new method is more reliable than the conventional method, and that the pull out displacement at the bottom of the wall is explained by more precisely measuring the strain in the reinforcement around the surface of the base slab.

### 4.3 Evaluation of Equivalent Damping

Equivalent damping value was evaluated using the applied load and each separate displacement according to the new method [Muroi et al, 1997] as shown in Figure 10. The new method is an expansion of the conventionally used method. The conventional equivalent damping [Jacobsen, 1960] is applied to the linear visco-elastic system under harmonic excitation, and is defined as the ratio of damping energy loss per cycle to the strain energy stored at maximum displacement. The new method can be applied to irregular cases; such where the origin of a loop shifts or the shape of the loop is extremely different on the positive and negative side because of the plastic deformation, as seen in Figure 10.

Equivalent damping values are evaluated for separate displacements. When the evaluated values are matched with the conditions of (1) damping over 16% ( $1/2\pi$ ), (2) damping negative and (3) loop twisted, those data are eliminated. Estimated equivalent damping for each separate displacement is shown in Figure 11, taking the equivalent damping as the ordinate and the drift angle of each component as the abscissa. Estimated damping values are classified into two groups. One is for a transient loop, which is the first cycle in each loading step, and the other is for stable loops, which comprise the remaining three cycles. Damping obtained from the transient loop comprises both hysteretic damping and hysteretic damping caused by plastic deformation, but damping obtained from stable loops comprises only hysteretic damping. Therefore, the discussion about Figure 11 focuses that from the stable loop as shown below.

For total horizontal displacement, damping from transient loop is scattered from 2 to 7%, and no clear tendency is observed. However, damping from the stable loop is distributed around 1~3%, and tends to increase with drift angle. Damping is distributed around 1 ~ 1.5% in the elastic range, where the drift angle is less

Table 3: Comparison of Curvatures Obtained from Vertical Displacement and Strain of Steel Bars of Web Wall

Unit is ( $\times 10^{-6}$  1/mm)

Load (kN)	Measured Curvature	Calculated Value1 <sup>*1</sup>		Calculated Value2 <sup>*2</sup>	
		Curvature	Ratio(%)	Curvature	Ratio(%)
9.8	-0.237	-0.222	93.87	-0.103	43.68
-9.8	0.163	0.236	145.21	0.108	66.21
19.6	-0.492	-0.460	93.56	-0.216	43.79
-19.6	0.441	0.502	113.95	0.216	48.87
39.2	-1.099	-0.987	89.82	-0.449	40.86
-39.2	1.058	1.007	95.14	0.373	35.23
58.8	-1.674	-1.480	88.42	-0.714	42.64
-58.8	1.719	1.657	96.42	0.647	37.62
78.5	-2.313	-1.958	84.64	-0.965	41.73
-78.5	2.627	2.487	94.68	0.983	37.44
98.1	-3.579	-2.869	80.17	-1.365	38.14
-98.1	4.109	3.638	88.53	1.491	36.27
117.7	-5.851	-5.015	85.71	-1.782	30.46
-117.7	6.352	5.563	87.58	2.671	42.05
137.3	-8.829	-7.078	80.17	-2.865	32.44
-137.3	8.960	7.312	81.61	3.691	41.19
156.9	-11.234	-8.134	72.40	-3.843	34.21
-156.9	11.538	8.473	73.43	5.024	43.54

\*1 : Estimated from 3 points measurement

\*2 : Estimated from 2 points measurement

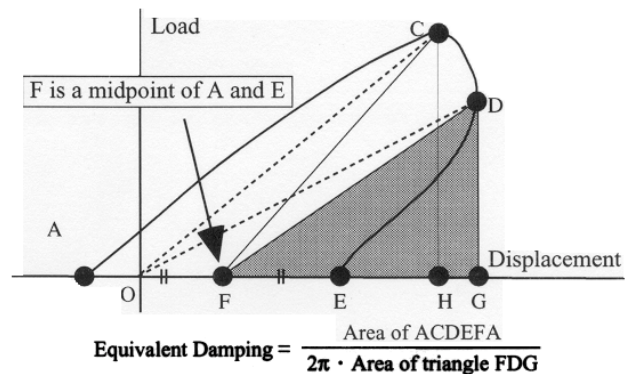


Figure 10: New Method to evaluate An Equivalent Damping

than  $0.25 \times 10^{-3}$ , and then increases and converges to 2% with the drift angle.

For shear displacement, the same tendency is shown as with total displacement. The damping value is about 1.5% in the elastic range, of which drift angle is less than  $0.23 \times 10^{-3}$ , and converges to a little over 2% around the second break point, where the drift angle is  $0.7 \times 10^{-3}$ .

For apparent flexure displacement, damping from the transient loop is distributed around 3 ~ 6% with some dispersion. However, for the stable loop, damping converges to around 2.5%.

For flexure displacement without rotation, damping from the transient loop is widely scattered, but that from the stable loop is distributed around 1% with one exception.

For rotation at the bottom of the wall, damping of the transient loop is widely scattered, but damping from stable loop is distributed around 4 ~ 5%, with a tendency to decrease with drift angle.

It becomes clear that damping of apparent flexure displacement contains the energy dissipation effect of the rotation at the bottom of the wall and is overestimated

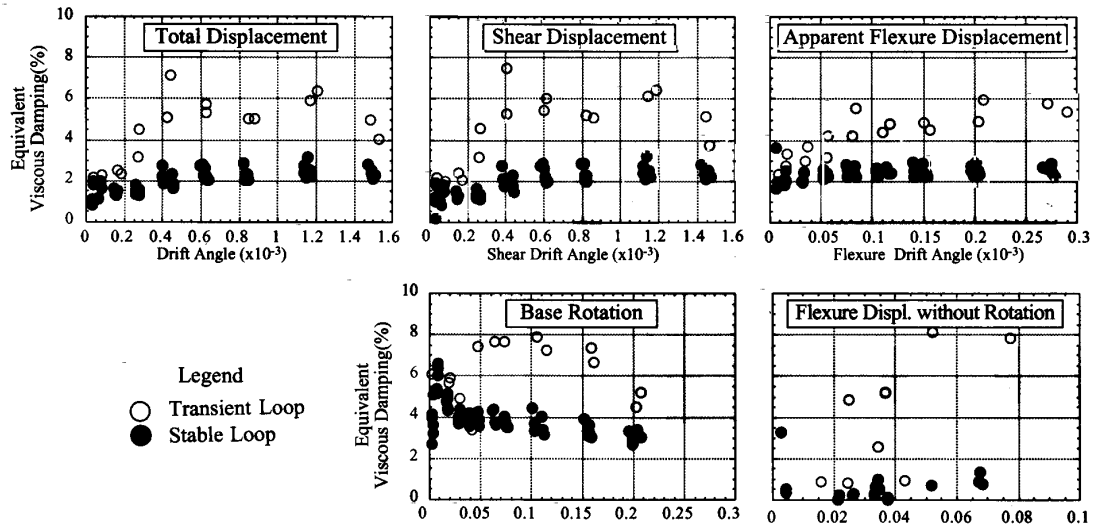


Figure 11: Relationship between Equivalent Damping and Separated Displacement Component

## 5. CONCLUSIONS

A precise static loading test on a RC shear wall has been conducted to evaluate the fundamental characteristics in the weak nonlinear range. The following conclusions were obtained from the test results and discussion.

- (1) The vertical displacement at the bottom of the flange wall consists not only of expansion or contraction of the flange wall but also of pull out displacement of the reinforcing bars from the foundation slab, and it is difficult to separate them. The displacement causes incorrect estimation of the flexure displacement. It is necessary to make the measurement as close as possible to the bottom of the flange wall to reduce the influence of displacement at the bottom of the flange on the total flexure displacement.
- (2) Precise measurement of strains in the reinforcing bars and displacements around the bottom of the flange wall makes it possible to evaluate the rotational displacement caused by the pullout of the reinforcing bars from the wall surface. As a result, the flexure displacement is estimated with good accuracy even in a large-scale model test.
- (3) The equivalent damping is very small in the elastic range, 0.5% for flexure deformation and 1.5% for shear deformation, which increases to 2% with increase in deformation.

Further study on the fundamental characteristics of the RC shear wall such as equivalent damping factor and the loading rate effects on stiffness and shear capacity in the weak nonlinear range will be conducted including the results of the dynamic tests.

## 6. REFERENCES

- JACOBSEN, L. S., (1960), "Damping in Composite Structures", *Proceeding of 2<sup>nd</sup> WCEE*, 41-1~41-16 Tokyo, Japan
- KANECHIKA, M., IGARASHI, K., MUROI, K. and AKINO, K. (1997) "Nonlinear dynamic analysis method for reinforced concrete shear wall of reactor buildings considering the strain rate effects on skeleton curves", *Journal of Structural and Construction Engineering (Transaction of AIJ)* No.495 May, pp107-114.
- MUROI, K., IGARASHI, K., SEKI, M., NAGASHIMA, T. and AKINO, K. (1997) "Dynamic restoring force characteristics of a reactor building Strain rate effects on the skeleton-curve for reinforced concrete shear wall", *Journal of Structural and Construction Engineering (Transaction of AIJ)* No.498 August, pp75-82.
- MUROI, K., INADA, Y., NAGASHIMA, T., KANECHIKA, M. and AKINO, K. (1997) "Dynamic restoring force characteristics of reinforced concrete shear wall in reactor building Energy dissipation capacity on plastic state and hysteresis model for dynamic analysis", *Journal of Structural and Construction Engineering (Transaction of AIJ)* No.501 November, pp65-72.
- OKADA, T., KANDA, J. and et all (1988), "Model tests for evaluation of the seismic behavior of reactor building part 1 ~ part 2", *Summary of technical papers of annual meeting architectural institute of Japan* October, No.2609-2610, pp1217-1220.
- OKADA, T., AKINO, K. and et all (1989), "Model tests for evaluation of the seismic behavior of reactor building part 3 ~ part 5", *Summary of technical papers of annual meeting architectural institute of Japan* October, No.2528-2530, pp1055-1060.
- SAKAI, A., KURIHARA, I., SHIRAISHI, I. and NAKAMURA, Y. (1992) "Studies on behavior of Reactor Building Walls Subjected to Large Earthquake Part1: Static and pseudo dynamic test of 3-D reinforced concrete shear wall", *Journal of Structural and Construction Engineering (Transaction of AIJ)* No.433 March, pp19-28.
- SHIBATA, A., KUBO, T., AKINO, K. and et all (1990), "Model tests for evaluation of the seismic behavior of reactor building part 6 ~ part 10", *Summary of technical papers of annual meeting architectural institute of Japan* October, No.2685-2689, pp1369-1378.
- SHIBATA, A., KANDA, J., KUBO, T., AKINO, K. and et all (1993), "Model tests for evaluation of the seismic behavior of reactor building part 11~part 14", *Summary of technical papers of annual meeting architectural institute of Japan* September, No.2780-2783, pp559-1566.
- SHIBATA, A., KANDA, J., KUBO, T., AKINO, K. and et all (1995), "Model tests for evaluation of the seismic behavior of reactor building part 15~part 16", *Summary of technical papers of annual meeting architectural institute of Japan* September, No.21506-21507, pp1011-1014.
- "Technical Guidelines for Aseismic Design of Nuclear Power Plants", *Translation of Japan Electric Association Guidelines (JEAG)*, 4601-1991, pp80-81 Tokyo, Japan